Carbon balance of a Finnish bog: temporal variability and limiting factors

Pavel Alekseychik[1,2], Aino Korrensalo[3], Ivan Mammarella[2], Samuli Launiainen[1], Eeva-Stiina Tuittila[3], Ilkka Korpela[5] and Timo Vesala[2,4]

[1] Bioeconomy and Environment, Natural Resources Institute Finland, 00791 Helsinki, Finland
[2] Institute for Atmospheric and Earth System Research/Physics, Faculty of Science, P.O. Box 68, FI-00014 University of Helsinki, Finland
[3] School of Forest Sciences, University of Eastern Finland, P.O. Box 111, FIN-80101 Joensuu, Finland
[4] Institute for Atmospheric and Earth System Research/Forest Sciences, Faculty of Agriculture and Forestry, P.O. Box 27, FI-00014, University of Helsinki, Finland
[5] Department of Forest Sciences, University of Helsinki, P.O. Box 27, 00014 University of Helsinki

Correspondence to: Pavel Alekseychik (pavel.alekseychik@luke.fi)

Abstract

Pristine boreal mires are known as substantial sinks of carbon dioxide (CO_2) and net emitters of methane (CH_4). Natural bogs constitute a major fraction of boreal mires. However, the bog CO_2 and CH_4 balances are poorly known, having been largely estimated based on discrete and short term measurements by manual chambers, and seldom using the eddy-covariance (EC) technique.

Eddy-covariance (EC) measurements of CO_2 and CH_4 exchange were conducted in the Siikaneva mire complex in southern Finland in 2011–2016. The site is a patterned bog having a moss/sedge/shrub vegetation typical of Eurasian southern Taiga, with several ponds near the EC tower. The study presents a complete series of CO_2 and CH_4 EC flux measurements and identifies the environmental factors controlling the ecosystem-atmosphere CO_2 and CH_4 exchange. A 6-year average growing season (May-September) cumulative CO_2 exchange of -60 g C m^{-2} was observed, which partitions into mean total respiration (Re) of 167 (146–197 annually) g C m^{-2} and mean gross primary production (GPP) of 228 (193–257 annually) g C m^{-2}, while the corresponding CH_4 emission amounts to 7.1 (6.4…8.4) g C m^{-2}. The contribution of October-December CO_2 and CH_4 fluxes to the cumulative sums was not negligible based on the measurements during one winter.

GPP, Re and CH_4 fluxes increased with temperature, and did not show a strong decline even after a substantial water table drawdown in 2011. Instead, GPP, Re and F_{CH4} became suppressed in cool, cloudy and wet conditions of 2012. May-September cumulative net ecosystem exchange (NEE) of 2013–2016 remained at about -73 g C m^{-2}, in contrast to the hot and dry year 2011 and the wet and cool year 2012, when suboptimal weather likely degraded the net sink by 20 and 40 g C m^{-2}, correspondingly. The cumulative growing season sums of GPP and CH_4 emission showed a strong positive relationship.

The EC source area was found to be comprised of 8 distinct surface types. However, footprint analyses revealed that contributions of different surface types varied only within 10–20% with respect to wind direction and stability conditions. Consequently, no clear link between CO_2 and CH_4 fluxes and footprint composition was found, despite the apparent variation of fluxes with wind direction.

1. Introduction

40   Natural mires are an important element of the Boreal and Arctic carbon cycle due to the vast amounts of carbon stored in peat, large area and their sensitivity to environmental changes (Gorham 1991, Charman et al. 2013). Over the last 10–14 thousand years, the northern mires have provided substantial climatic cooling (Frolking and Roulet 2007). It is expected, however, that the rising air temperature will likely drive an increase in the emission of methane (CH_4) (Zhang et al. 2017) and carbon dioxide (CO_2) (Laine et al. 2019). As the effects of rising temperature are strongly dependent on water table level (Davidson and

45   Janssens 2006, Buttler et al. 2015, Laine et al. 2019), the precipitation extremes in northern latitudes (IPCC 2013) will contribute to the variability and uncertainty of any predictions. Pristine bogs, i.e. primarily rain-fed, oligotrophic peatlands with a developed microtopography and often populated by trees, constitute a major and diverse class of boreal mires (Seppä 2002). The response of their GHG balances to the environment is therefore of utmost interest. The complex surface patterning of a bog and the need for continuous measurements favours the application of area-integrating eddy-covariance (EC) measurements (Baldocchi 2008),

50   a technique providing an estimate of vertical net flux of scalars and heat over a large (~1–100 ha) source/sink area (flux footprint) that typically envelops all representative microsites. However, because most boreal bog GHG balance estimates to date were produced by chambers or short campaign-based EC studies, the magnitude and controls of CO_2 and CH_4 flux inter-annual variability are still poorly known. The strong ecological diversity of bogs is reflected in the previous bog eddy-covariance studies, which examined a temperate wooded bog (Fäjemyr; Lund et al. 2007, Lund et al. 2012), temperate shrub bog (Mer Bleu;

55   Lafleur et al. 2001, Lafleur et al. 2005, Roulet et al. 2007, Brown 2014), boreal treed/low shrub bog (Attawapiskat river; Humphreys et al. 2014), boreal shrub bog (Kinoje Lake; Humphreys et al. 2014), boreal raised bog (Tchebakova et al. 2015), boreal collapse scar bog (Bonanza Creek Experimental Forest; Euskirchen et al. 2014), boreal raised patterned bog (Mukhrino; Alekseychik et al. 2017), temperate patterned *Sphagnum*/shrub bog (Arneth et al. 2002), boreal open patterned bog (Arneth et al. 2002). Due to such a broad range of vegetation and climate, identifying the "typical" bog GHG balance and its environmental

60   controls presents a certain challenge.

The previous EC and chamber estimates indicate that boreal bogs typically demonstrate a small to moderate annual sink of CO_2 and a relatively small source of CH_4 (on a level similar to fens). The annual (or growing season) net CO_2 exchange in bogs across the entire boreal region varies typically from +30 to -100 g C m^{-2} a^{-1} (e.g. Tchebakova et al. 2015, Lund et al. 2010, Roulet et al. 2007, Lafleur et al. 2003), which splits into gross primary productivity (GPP) and ecosystem respiration (Re) both

65   typically in the range of 200–500 g C $m^{-2} a^{-1}$. The fairly wide spread in these numbers is attributed to the variation in site-specific (vegetation, hydrology, peat structure) and external (climate, weather) factors. Studies extending over several years reveal that bog CO_2 balance is sensitive to temperature and water table level (WTD) (Lafleur et al. 2003). Hot and dry weather suppresses bog photosynthesis and promotes respiration (Alm et al., 1999; Lund et al., 2012, Euskirchen et al. 2014, Arneth et al. 2002, Tchebakova et al. 2015, Lund et al. 2012). Under favourable conditions, which seem to consist of warm temperatures, ample

70   sunshine, sufficient moisture but no long-term WTD rise, bogs can show a high growing season net CO_2 uptake of 100–200 g C m^{-2} (e.g. Friborg et al. 2003, Alekseychik et al. 2017).

In wetlands, the total methane emission is a sum of diffusion through soil matrix, ebullition and plant transport, each associated with a set of environmental controls (Lai 2009). Peat temperature is known to be the primary driver of CH_4 production (e.g. Dunfield et al. 1993). About 50–90% of the produced methane is oxidized in the oxic zone before it can reach the atmosphere

75   (King et al. 1990, Fenchner and Hemond 1992, Whalen and Reeburgh 2000), so WTD is potentially an important driver. While bogs are expected to conform to these general dynamics, it would be interesting to improve the knowledge on the effective CH_4 emission that results from their specific structure.

At present, the lack of multi-year eddy-covariance studies in boreal bogs does not allow to rank the environmental controls by their importance for CH_4 emission. It was previously observed that nothern bogs typically emit from 0 to 20 g C m^{-2} annually in

80   the form of methane (Vompersky et al. 2000, Friborg et al. 2003, Roulet et al. 2007). The bogs with developed ridge-hollow microtopography were identified as the mire types with the highest CH_4 emission spatial variability in western Siberia (Kalyuzhny et al. 2009); a high spatial heterogeneity was also found in a Canadian bog study (Moore et al. 2011)

The available shorter datasets from bogs, and the more abundant data from fens, do shed some light on the possible controls. Methane net efflux (F_{CH4}) is strongly correlated with GPP; to which extent this is due to accelerated rhizospheric CH_4

85   production as a result of photosynthate input or enhancement of CH_4 transport by vascular plants is not clear (Bellisario et al. 1999, Rinne et al. 2018). The water table depth (WTD) control is equally unclear, with reports of existence of an optimum WTD (e.g. Rinne et al. 2018) and limitation of CH_4 efflux due to WTD lowering (Glagolev et al. 2001, Kalyuzhny et al. 2009). Euskirchen et al. (2014) show that only a drought or considerable strength is able to limit bog CH_4 emission. CH_4 Ebullition ebullition is prompted by drops in atmospheric pressure but is reduced by rapid peat temperature drops (Fechner-Levy &

90   Hemond 1996).

The EC technique is usually assumed to provide flux estimates representative of the studied ecosystem (e.g. Aubinet et al. 2012). However, in heterogeneous sites this may not be the case. The bog surface cover heterogeneity has several characteristic spatial scales, including vegetation community (1 m^2), microsites, e.g. hummocks and hollows (1–10 m^2), and larger formations, such as ponds and ridges (50–1000 m^2). These surface elements have been shown to have significantly different surface-atmosphere

95   GHG exchange rates (Alm et al. 1999, Repo et al. 2007, Maksuytov et al. 2010, Kazantsev and Glagolev 2010). In order to understand the output of EC system in such a heterogeneous site, one needs to estimate the contributions of the surface cover types to the total flux. The EC flux is strongly influenced by sources from near the tower (Vesala et al. 2008), but also by the larger scale general surface composition in different wind direction sectors. How much the resulting footprint variation affects the EC data has be analyzed in detail (e.g. Tuovinen et al. 2019).

100   In the present study, we report six years of CO_2 and CH_4 fluxes measured by EC at a raised patterned bog area of the Siikaneva mire, Southern Finland. The long-term data is used to analyze the responses of bog-atmosphere CO_2 and CH_4 exchange to environmental forcing during growing season (May-September), and to provide growing season balances. Specifically, we aim to:

1)   Quantify CO_2 and CH_4 balances of a boreal bog ecosystem on seasonal and annual timescales;

105   2)   Identify the environmental controls responsible for seasonal and inter-annual variability of the carbon exchange;

3)   Explore whether signals from surface type heterogeneity within the footprint can be detected in the observed CO_2 and CH_4 fluxes.

2. Materials and methods

2.1 Site description and previous research

110   The Siikaneva-2 site (61.8° N, 24.2° E) is situated in a patterned ombrotrophic bog within the larger Siikaneva mire complex in Southern Finland (Fig. 1). The site microtopography is dominated by rows of hummock strings (Figure 1). The areas with lower elevation are considerably varied, being composed of hollows and lawns, moss-free mud bottoms and ponds. The dominating moss species are *Sphagnum rubellum*, *S. papillosum*, *S. fuscum*, while the most widespread vascular plants are *Rhynchospora alba*, *Andromeda polifolia*, *Calluna vulgaris* and *Rubus chamaemorus*; a few small Scots pines (*Pinus sylvestris*) grow on the

115   ridges. The pond depths range from 0 to 2 m. The temporal variations in the bog water level lead to the variation in pond size and

occasionally result in inundation of the mud bottoms. The 4-year average (2012-2015) peak total vascular plant leaf area index (LAI) was 0.35 m^2 m^{-2} and the peak aerenchymous LAI was 0.24 m^2 m^{-2}. Details on microform types and vegetation composition is given in Korrensalo et al. (2016) and Korrensalo et al. (2017).
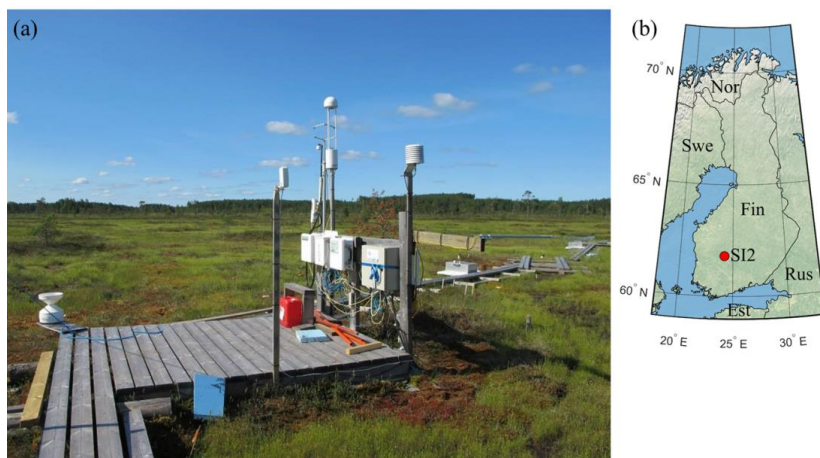
Figure 1: (a) Photo of the eddy-covariance tower and meteorological setup facing south-west. (b) Map of Finland showing the location of the Siikaneva-2 site.

The site is highly heterogeneous due to the patchy vegetation cover. The western sector of the EC footprint is dominated by ponds, hollows and lawns, while in the eastern sector one encounters several well-defined ridges. The nearest forest edge lies in 150 m NE of the EC tower.

2.2 Measurements

2.2.1 Eddy-covariance measurements

EC measurements of CO_2, CH_4, sensible and latent heat fluxes were conducted at the site in the years 2011–2016 using a METEK USA-1 anemometer, a LiCor LI-7700 open-path CH_4 analyzer, and a LiCor LI-7200 enclosed path CO_2 & H_2O analyzer mounted at 2.4 m height above the peatland surface. The EC raw data were processed using EddyUH software (Mammarella et al., 2016) following standard schemes and quality control protocols (Nemitz et al. 2018, Sabbatini et al. 2018). The CH_4 fluxes at Relative Signal Strength (RSSI) < 20 were excluded from analysis. A friction velocity (u_*) filter of 0.1 m s^{-1} was applied based on the observed behavior of the normalized CH_4 and CO_2 fluxes under low turbulence conditions. Fig. 2 shows the normalized CH_4 and CO_2 fluxes and the energy balance closure plotted against u_*. Interestingly, while the normalized GHG fluxes both saturate at $u_* = 0.1$ m s^{-1}, the energy balance closure does so only at u_* above 0.15 m s^{-1}. See Table 1 for the proportion of the 30-min average CO_2 and CH_4 fluxes remaining after quality control and u_* filtering.
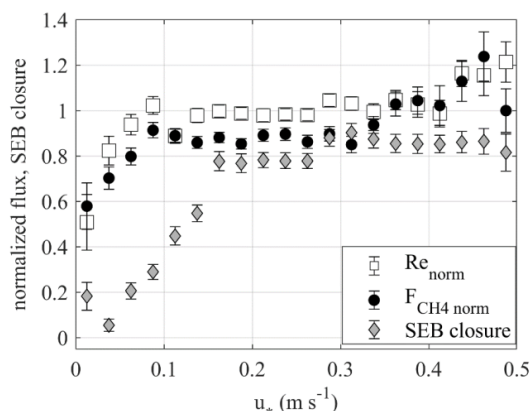
Figure 2: Bin-median values of CO_2 respiration (Re) and CH_4 efflux, normalized by their temperature-based statistical models, and surface energy balance closure (SEBC = (H + LE) /R_n) *versus* friction velocity for May-October, with the bars giving STD of the median.

Table 1: Fraction of 30-min EC fluxes of CO_2 and CH_4 remaining after the quality checks and u_*-filtering, in % of the specified period.

	May-September		June-August	
	F_{CO2}	F_{CH4}	F_{CO2}	F_{CH4}
2011	27	21	41	33
2012	63	44	55	33
2013	18	37	24	34
2014	52	43	72	57
2015	45	40	59	51
2016	53	31	75	45
average	43	36	54	43

2.2.2 Auxiliary measurements

Meteorological and environmental measurements were made next to the EC tower. Peat temperature (T_p) profile was measured by Campbell 107 Thermistor sensors at 5, 20, 35 and 50 cm depths since July 2011. In April 2012, the auxiliary measurements were expanded with net radiation sensor Kipp & Zonen NR Lite2, air temperature (T_a) and relative humidity (RH) sensor Campbell CS215, WTD sensor Campbell CS451 and tipping bucket rain gauge ARG-100. The peat temperature profile and the water table sensor were installed in a lawn microform near the EC tower.

The peat temperature at 20 cm depth (T_{p20}) and WTD were gap-filled using regressions with the data from the Siikaneva-1 fen station (SI1, Rinne et al. 2007, Rinne et al. 2018) 1.2 km SE from the site. Measurements from the SMEAR-II station (Hyytiälä, 7 km away) were used to gap-fill T_a and RH and supply the complete timeseries of photosynthetic active radiation (PAR).

155   Precipitation rate time series was constructed as a combination of observations at SMEAR-II site and Finnish Meteorological
        Institute weather station (Hyytiälä).

        A campaign for leaf area index (LAI) measurement was undertaken at the site in 2012–2015. The representative microforms
        were covered by three replicate plots 60 x 60 cm in size, 18 in total. Within each plot, five small subplots were defined for the
        manual measurement of leaf number. This measurement was made approximately twice a month throughout the growing season,

160   and simultaneously, average leaf size of each species was defined with a scanner. To obtain the leaf area of the subplots, the leaf
        number was multiplied by the average leaf area. These community-specific LAI were then averaged and weighted by their area
        fractions within EC footprint to yield the ecosystem-scale value (Korrensalo et al. (2017). The years of 2011 and 2016, when
        LAI was not measured, were filled with the 2012–2015 average LAI.

2.2.3. Aerial imaging

165   A survey including Lidar scanning and aerial photography was conducted by helicopter in May 2013. The data at the original
        resolution of 4 cm/pixel were processed and converted into a surface cover type map and a digital elevation map (Figure 3). As
        the individual microforms measure in area roughly 1–2 m^2, and in order to mitigate the motion blur present in the images, the
        resolution of all maps was coarsened to 1 m^2/pixel.
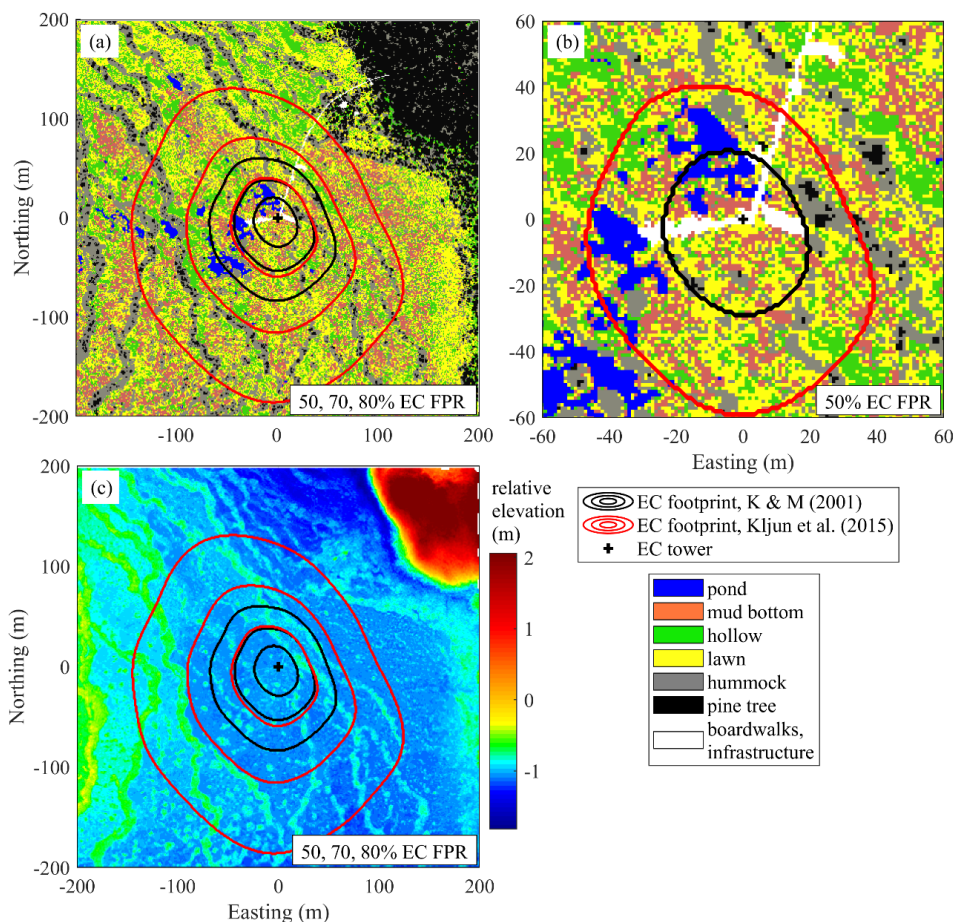
170 **Figure 3:** Site characteristics obtained from the helicopter survey in May 2013. a) Surface cover map at 1 m resolution showing a 400 x 400 m patch of landscape centered on the EC tower. The cumulative Kormann & Meixner (2001) and Kljun et al. (2015) flux footprints are given by 50, 70 and 80% contribution contours. b) Close-up map, focusing on the 50% cumulative footprint zones. c) Digital elevation model derived from Lidar scan. Note that the 70% Kljun et al. (2015) isoline coincides with the 50% Kormann & Meixner (2001) isoline.

175

The proportion of each microform for the whole extent of the map (400 x 400 m, centered on the EC tower) and their proportions weighted by the two footprint models were roughly similar (Table 2). However, due to the proximity of the EC tower to the ponds (as was intended on the site planning stage) and boardwalks, their proportions are comparatively higher than in the greater area. The boardwalks extending in the western and eastern directions from the EC tower raft were built in April-June 2012, after

180 the first measurement season. Also note that when the boardwalks some 30–40 cm wide are rescaled to the resolution of 1 m, their area becomes artificially exaggerated.

Table 2: Proportions of the surface types and microforms, expressed as area percentage (first column) or weighted by the cumulative footprints, Kormann & Meixner (2000) and Kljun et al. (2015) (second and third columns).

185

	Areal cover (%) within the entire map (200 x 200 m)	Contribution (%) for K&M cumulative footprint within 80% contribution zone	Contribution (%) for Kljun cumulative footprint within 80% contribution zone
pond	2.3	7.7	9.1
mud bottom	15.3	19.7	24.2
hollow	18.8	14.4	10.3
lawn	27.3	27.3	26.3
high lawn	7.1	6.9	7.0
hummock	10.5	10.5	9.6
high hummock	18.3	8.2	5.5
boardwalks	0.4*	5.3*	8.0*

*overestimate

2.3 EC flux footprint modeling

EC scalar flux footprints were calculated using the widely used Kormann & Meixner (2001) and Kljun et al. (2015) models. The footprint lengths are very dependent on roughness length z_0, necessitating its careful calculation. The 30-min average values of z_0

190 were calculated using the formula

$$z_0 = z \exp\left(\frac{-\kappa U}{u_*} - \psi_m\left(\frac{z}{L}\right)\right),$$

(1)

Where $\psi_m(z/L)$ is the stability correction function defined, following Beljaars & Brutsaert (1991), as

195

$$\psi_m = 2\log\left(\frac{1+x}{2}\right) + \log\left(\frac{1+x^2}{2}\right) - 2\arctan x + \frac{\pi}{2} \qquad \left(\frac{z}{L} < 0\right)$$

(2)

$$\psi_m = -A\frac{z}{L} - B\left(\frac{z}{L} - \frac{c}{d}\right)\exp\left(-d\frac{z}{L}\right) - \frac{bc}{d} \qquad \left(\frac{z}{L} > 0\right)$$

(3)

200   with A = 0.7, B = 0.75, c = 5 and d = 0.35. Instantaneous z_0 values were used to model the footprint for each 30-min period so that to account for the rapid variation in z_0 due to the changing stability conditions and directional variation in surface roughness. We note that it was necessary to filter the calculated 30 min z_0 values for very stable nocturnal conditions, which initiate a decoupling phenomenon. At nighttime thermal decoupling, which in Siikaneva typically happens below the EC measurement height (unpublished data), spikes in U/u_* are observed which can be interpreted as airflow losing contact with the surface;

205   therefore, the z_0 values at $U/u_* > 12$ and/or $u_* < 0.1$ m s^{-1} were eliminated. High instantaneous z_0 values may also occur at strongly convective conditions, when high instability is combined with low wind speeds, but those values are retained, with only the extreme values $z_0 > 3$ m being excluded. The z_0 remaining after such filtering were from 0 to 3 m, with 80% of the values being between 0 and 0.1 m and the most probable value being 0.03 m. The displacement height was set to zero as the surface roughness elements are small and sparse.

210   Footprint estimates were calculated on a 1 x 1 m grid in order to match the resolution of the surface cover map. The footprint nodes lying further than 200 m away from the origin (coinciding with the location of the EC tower) were eliminated. Such as exclusion of the map corners was necessary since, should they have been preserved, there would have been a bias between the footprints extending towards the corners and those extending in N, E, S and W directions due to the difference in the number of nodes. Finally, since a fraction of the EC signal (roughly 10-20%) comes from beyond a 200 m distance from the tower, all

215   footprint values within this domain were normalized by their cumulative sums.

2.4 Modeling the CO$_2$, CH$_4$ fluxes and EC flux gap-filling

The EC fluxes were modeled and gap-filled using the method similar to that in Alekseychik et al. (2017). The resulting models were used to fill the gaps in measured fluxes during the May-September period. Respiration and photosynthesis were represented with the familiar Q$_{10}$ and Micaelis-Menthen-type expressions,

220

$$Re_{mod} = Re_{ref}\, Q_{10\,CO2}^{\left(\frac{T_{p5}-12}{10}\right)}$$

(4)

$$GPP_{mod} = \frac{P_{max}PAR}{k+PAR}.$$

(5)

225   Methane emission was given a similar formulation as Re,

$$F_{CH4mod} = F_{ref}\, Q_{10\,CH4}^{\left(\frac{T_{p20}-12}{10}\right)}$$

(6)

T_{p20} was chosen as the driver of F_{CH4} as it performed slightly better than T_{p5} in terms of model R^2, RMSE and SSE. A reference

230 temperature of 12˚C was used for both Re and F_{CH4} (Eqs. 4 and 6), as representative peat temperature at the site.

Given the presence of both short and long data gaps in the measured fluxes, the following gap-filling method was adopted after some trials:

1)   General-fit models of Re and F_{CH4}: The Q_{10} for Re and F_{CH4} were estimated from a single fit to all data; the median fluxes calculated in temperature bins were used on this step in order to reduce the random uncertainty and uneven distribution of

235 the 30-min fluxes in different temperature ranges.

2)   Sliding-window models of GPP, Re and F_{CH4}: Another set of models was constructed by fitting Eqs. 4-6 in sliding time windows of 15 days wide for Re, 10 days for GPP, and 5 days for F_{CH4}. The resulting daily values of P_{max}, k, Re_{ref} and F_{ref} were linearly interpolated to each 30min period. Extrapolation beyond the EC measurement periods in each year was not done. The resulting 30-min parameter time series were used to model the instantaneous Re, GPP and F_{CH4}.

240 3)   While the models obtained on the previous step imitate the behavior of the measured data well, they show a poor prognostic performance during long gaps or beyond the flux measurement period. This is particularly relevant for GPP, which is strongly related to vegetation phenology. The parameters of statistical models cannot be safely extrapolated to the longer gaps in measured data, therefore, they had to be gap-filled with the constant values estimated from a fit to all available data. This concerns mainly the edges of the growing season. As preliminary tests revealed the potential importance of peat and air

245 temperature and LAI, three models were tested: (i) GPP = f(PAR,$T_{p\,5cm}$) fit to all data, (ii) GPP = f(PAR, LAI, T_a) fit to all data, (iii) GPP = f(PAR, LAI, T_a) fit separately for each year. The model (i) showed a clearly superior performance in terms of residuals, RMSE and the width of parameter confidence intervals. Correspondingly, the expanded GPP expression is now:

$$GPP_{mod} = \frac{P_{max}PAR}{k+PAR}\left(aT_{p\,5cm} + b\right) \qquad (7)$$

250

Eq. 7 was fit to all quality-controlled data to determine P_{max}, k, a, and b. Effectively, the Re, GPP and F_{CH4} models used for gap-filling are ultimately combinations of two types of model: sliding fit models during short gaps, and general-fit models during long gaps.

3 Results and discussion

255 **3.1 Environmental conditions**

The climate is south boreal, with the mean 30-year average annual precipitation (liquid equivalent) of 711 mm and air temperature 3.5 ˚C (Table 3). The summer is typically warm and relatively dry, having a 30-year average air temperature of 14.6 ˚C and precipitation of 252 mm. The weather in the six measurement years represents a range of conditions from warm/dry/sunny to cool/moist/cloudy (Fig. 4). Most of the years were warmer and drier than the 30-year average. Fig. 5 shows

260 the seasonal variation in the main environmental drivers. The year 2012 was atypical due to its low temperatures and ample precipitation, whereas another cool year 2015 had a sunny but dry autumn and an early drop in LAI (Fig. 5 g, h). Normalized LAI was rather similar in the rest of the study years. 2011 had an untypically dry spring and summer, which resulted in the lowest mean summertime WTD of -20 cm. The dry conditions of 2011 were also evident in the sharply increased diurnal amplitude of the peat temperature at 5 cm depth, implying the top peat layer and moss capitula were potentially desiccated. The

265 maximum average growing season WTD of -7 cm was observed in 2012 (Fig. 5e).

Table 3: Average annual and summer air temperature, liquid water equivalent precipitation and water table depth in comparison with the 30-year averages.

Period	Annual		June-August		
	T_a	precip.	T_a	precip.	WTD
	(°C)	(mm)	(°C)	(mm)	(cm)
2011	5.2	777	16.6	261	-20
2012	3.3	925	14.1	310	-7
2013	5.1	632	15.9	240	-15
2014	5.0	642	15.7	314	-12
2015	5.6	678	14.3	230	-11
2016	4.4	784	14.8	356	-10
long-term	3.5 [a]	711 [a]	14.6 [a]	252 [a]	-12 [b]

270

[a] 1981-2010, Pirinen et al. (2012)

[b] The average of 2011–2016, as no longer-term data exist.
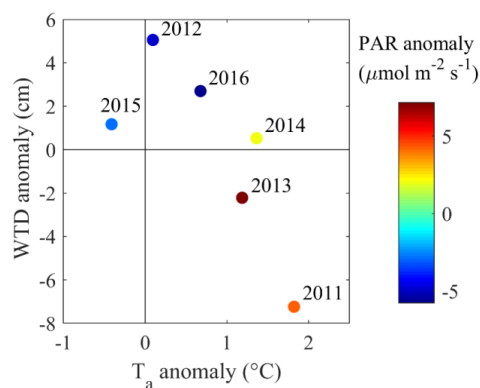
275   **Figure 4:** June-August deviations in water table depth, air temperature and PAR, calculated as difference from the 6-year averages for WTD and PAR and 30-year averages for T_a.
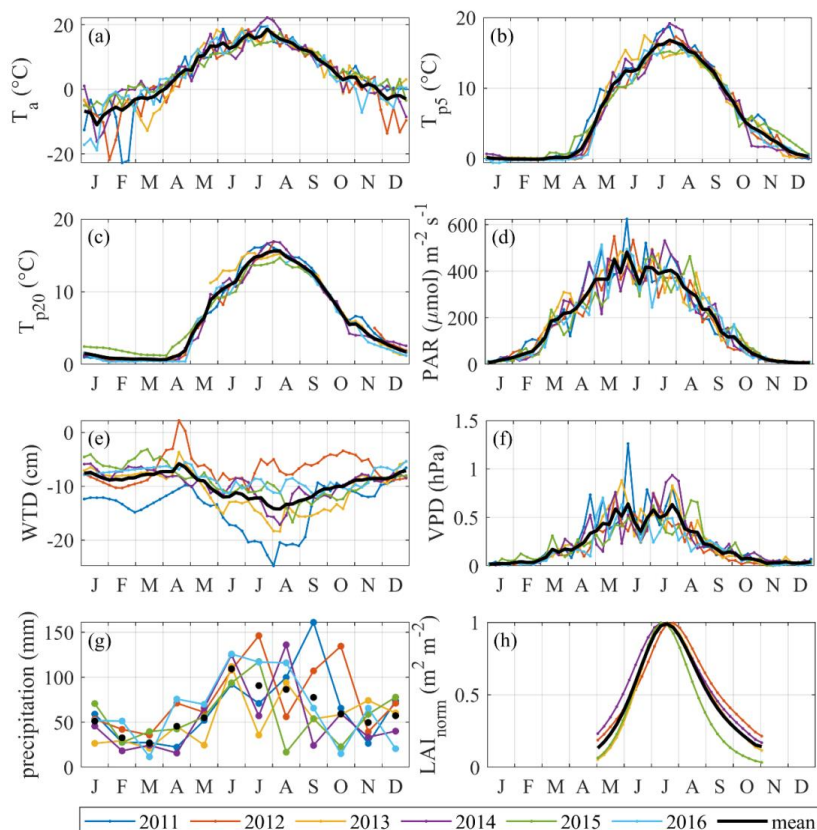
Figure 5: Time-series of potential drivers of NEE, GPP, Re and F_{CH4}. LAI is normalized by the annual peak value. The color lines in (a), (b), (c), (d), (f) represent weekly means, whereas in (e, h) they give daily average WTD and in (g) monthly precipitation sums. The black lines in (a–f) show the mean annual course of all years; the black markers in (g) are the monthly average precipitation of all years.

3.2 Parameters of the CO_2 and CH_4 flux models

The fitting of Eqs. 4, 6 and 7 to all available data produced the Re, GPP and F_{CH4} model parameter values that are summarized in Table 4.

Table 4: Parameters of the fits for Re, GPP and F_{CH4} made using all quality-controlled data. The 95% confidence intervals are given in parentheses.

Re (Eq. 4)	R_{ref} (µmol CO_2 m⁻² s⁻¹) 0.73 (0.68…0.78)	$Q_{10\ CO2}$ 3.39 (2.87…3.90)
F_{CH4} (Eq. 6)	F_{ref} (µmol CH_4 m⁻² s⁻¹) 0.038 (0.037…0.040)	$Q_{10\ CH4}$ 4.91 (4.43…5.39)
	P_{max} 4.40 (4.39…4.41)	k 222 (199…245)

11

GPP (Eq. 7)

a	**b**
0.074 (0.070…0.078)	-0.10 (-0.15… -0.06)

290

3.3 Seasonal variability in the CO_2 and CH_4 fluxes

Flux time series over the study period are shown in Fig. 6. The measurements were mostly conducted during the growing season, with some autumn and winter periods covered in 2011–2012 and 2014–2015. Both the CO_2 and CH_4 fluxes are at their highest during the growing season from May to September. While the seasonal curve NEE does not appear to show a marked deviation

295 from dome over the growing season, its daily variation responded strongly to environmental conditions on a weekly to biweekly scale, with the beneficial conditions resulting in peak daily mean NEE of about $-1…-1.5$ μmol m^{-2} s^{-1}, and poor weather reducing that to zero. The seasonality of the partitioned CO_2 fluxes varied markedly between the years. 2011 and 2014 yielded higher seasonal peaks in GPP and Re than in the other years, corresponding with the periods of warmest weather. Maximum GPP reached 4.3–4.5 μmol m^{-2} s^{-1} in 2011 and 2014, which is substantially higher than 3.0–3.1 μmol m^{-2} s^{-1} observed in the other

300 years. Correspondingly, the maximum daily mean respiration reached 3.5 μmol m^{-2} s^{-1} in 2011 and 2.7 μmol m^{-2} s^{-1} in 2014, while the other years showed 1.6–1.9 μmol m^{-2} s^{-1} at the peak. The summer peaks in CH_4 flux in 2011 and 2014 closely matched those in GPP and Re and also resulted in the highest daily averages reaching 0.1 μmol m^{-2} s^{-1}. In the other years, CH_4 flux daily means reached 0.07–0.08 μmol m^{-2} s^{-1} with an overall smoother seasonal maximum.

The importance of the non-growing season fluxes was also analyzed. The spring peak of CH_4 emission associated with the thaw

305 period in April and May contributes only a minor, although non-negligible fraction of spring-summer total. In 2012, elevated net emission lasted for about 8 days (25 April–3 May), and in 2013, 10 days (22 April–5 May). These periods supplied roughly 4% of the cumulative CH_4 emission of 25 April – 31 August 2012 and 22 April – 31 August 2013. Based on partially covered winters of 2011-2012 and 2014-201, the cumulative wintertime season fluxes were relatively small but non-negligible as well. In 2011, the Oct–Nov contributions to May-Nov cumulative fluxes were as follows: 12% for F_{CH4}, 4% for GPP, and 8% for Re. In

310 2015, the corresponding values were 14%, 5% and 13%. Finally, in 2014, Oct–Dec contributed 10% of F_{CH4}, 4% of GPP, and 13% of Re to the May–December totals.
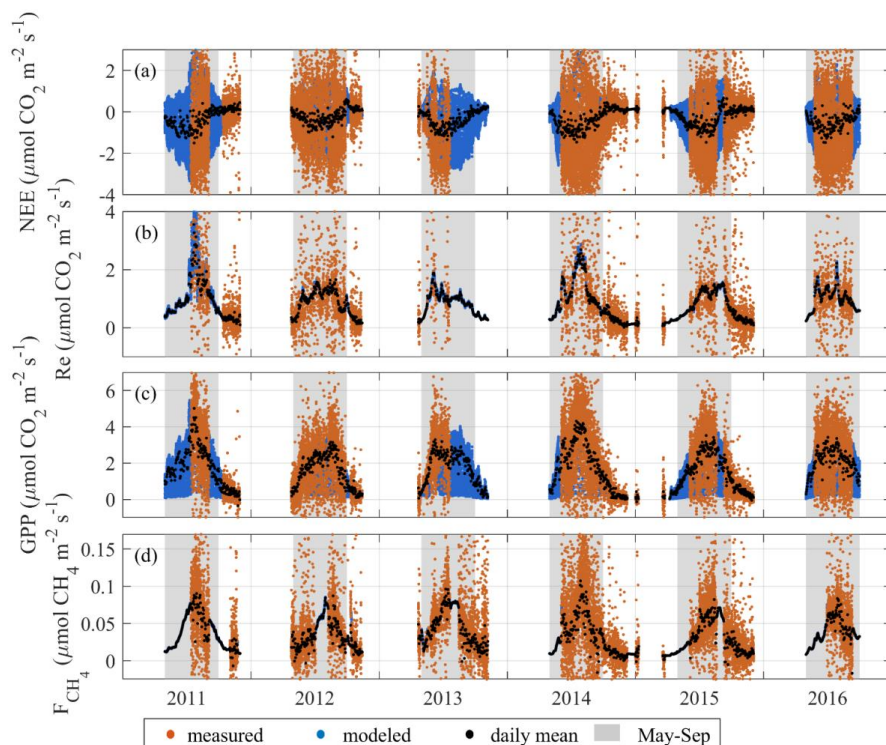
Figure 6: Timeseries of measured and modeled 30 min values of NEE, Re, GPP and F_{CH4}. The gray shading highlights the growing season (May-September). The model CH_4 flux 30 min values are mostly hidden under the daily mean markers.

3.4 Drivers of the seasonal variation in CO_2 and CH_4 fluxes

Figure 7 shows the temporal course of NEE, GPP, Re and F_{CH4} model parameters (Eqs. 4–7) and reveals both their well-defined seasonalities and interannual differences. The CH_4 reference flux has pronounced maxima in April and October-November (Fig. 7a), when the emissions may have been dominated by ebullition which is not controlled by temperature (so that high efflux coincided with low peat temperature). Between June and September, F_{ref} falls on average from 0.045 to 0.035 μmol CH_4 m^{-2} s^{-1}. Re_{ref} (Fig. 7b) peaks in May at 1.2 μmol CO_2 m^{-2} s^{-1}, stagnates for the rest of the growing season, and thereafter gradually drops to about 0.5 μmol CO_2 m^{-2} s^{-1} by December. However, this behavior is again detectable only in the monthly averages. k and P_{max} (Fig. 7c,d) have a broad maximum in the middle of the growing season, more pronounced in P_{max} than in k.
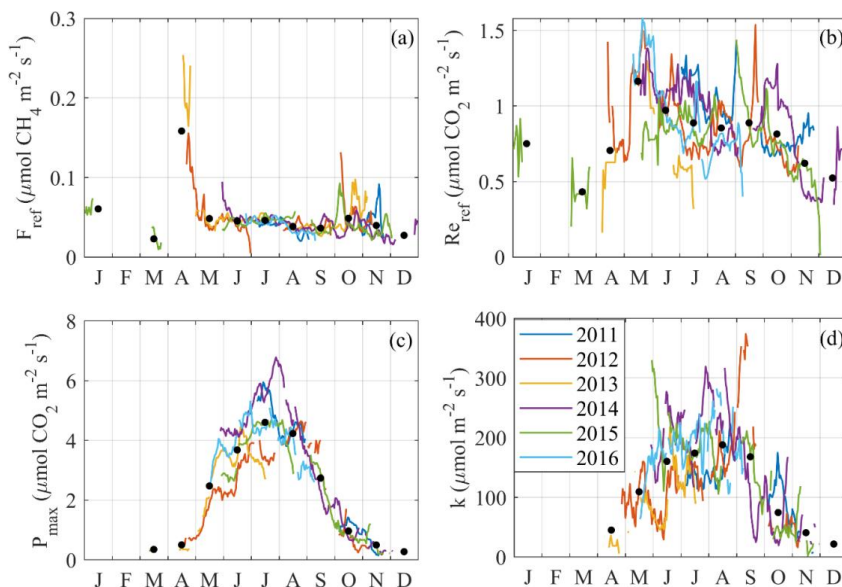
Figure 7: Time series of CO_2 and CH_4 flux model parameters (Eqs. 4–6): (a) Re_{ref}, (b) F_{ref}, (c) P_{max}, (d) k. Monthly averages
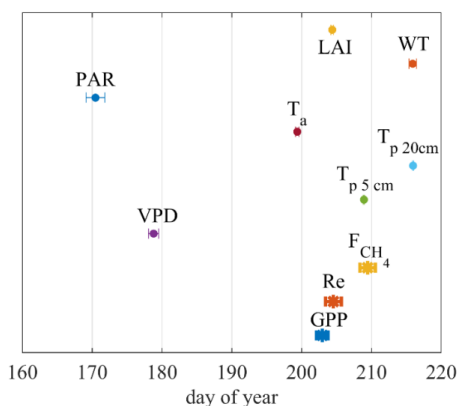across years are shown with black dots.

Figure 8: Day of year corresponding to the annual peaks in fluxes and their potential drivers. The bars give the 95% parameter
CI.

The timing of seasonal maxima in fluxes and environmental drivers were explored by fitting the Gaussian function to GPP, F_{CH4}
Re and their physical drivers (log-linear function for LAI_{norm}, Wilson et al. 2007), regressed against the day of year. The mean
seasonal peak was estimated as the peak of the fit curves (Fig. 8). The peaks so derived mostly fall between the days 199 and
216, except those of VPD and PAR that occur on the days 171 and 178, respectively.

3.4.1 The effect of footprint variation

In heterogeneous mires, the variation in the EC footprint, controlled by wind direction and stability, may contribute to flux
temporal variability, complicating the interpretation (Tuovinen et al. 2019). Curiously, the two models, Kormann and Meixner

(2000) and Kljun et al. (2015), produce quite similar surface compositions despite the significant difference in footprint length (Fig. 9). The variations in stability did introduce some variation in the footprint zone elongation, but did not cause significant
340 changes in the footprint composition. The footprint composition, however, varied with wind direction, as the contributions of some microforms did vary among the wind direction sectors. The pond contribution ranges from zero to about 20%, being the most significant change, while the share of the other microforms varies by about 10%.
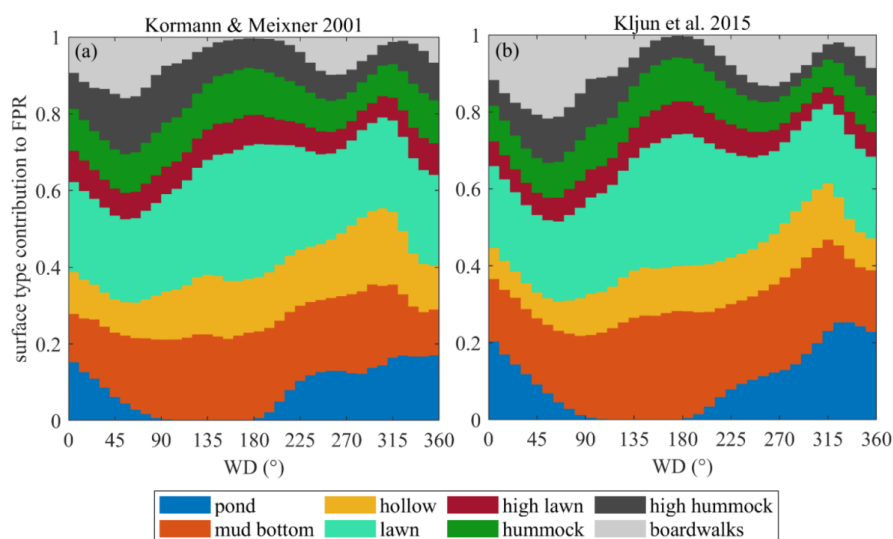
Figure 9: Surface type contributions to surface exchange versus wind directions, presented as means over 10° WD bins using all available data.

The question whether the directional variation in footprint composition has a noticeable effect on CO_2 and CH_4 fluxes is addressed in Fig. 10 that presents both the measured fluxes and the reference flux obtained by moving-window modeling. The
350 relative variation in the reference fluxes is broad, being about 60% in Re_{ref}, 40% in P_{max} and 20% in F_{ref} (Fig. 10a), with the measured fluxes showing a similar directional variation (Fig. 10b). Importantly, in the western sector, roughly corresponding to the highest pond contribution, P_{max} and Re_{ref} are at their minimum while the F_{ref} is at its maximum.
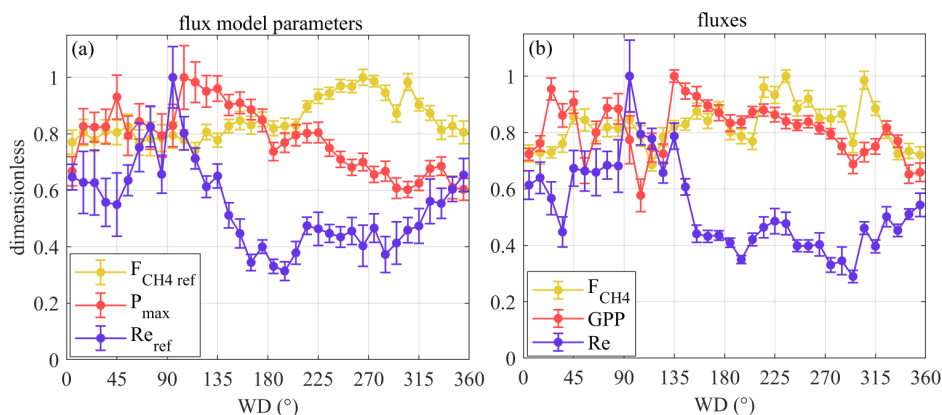
Figure 10: Variation of June-August fluxes and flux model parameters with wind direction. a) Variation in the CO_2 and CH_4 flux model parameters, b) measured fluxes. The markers are bin-averages normalized by the highest bin-average value for clarity.
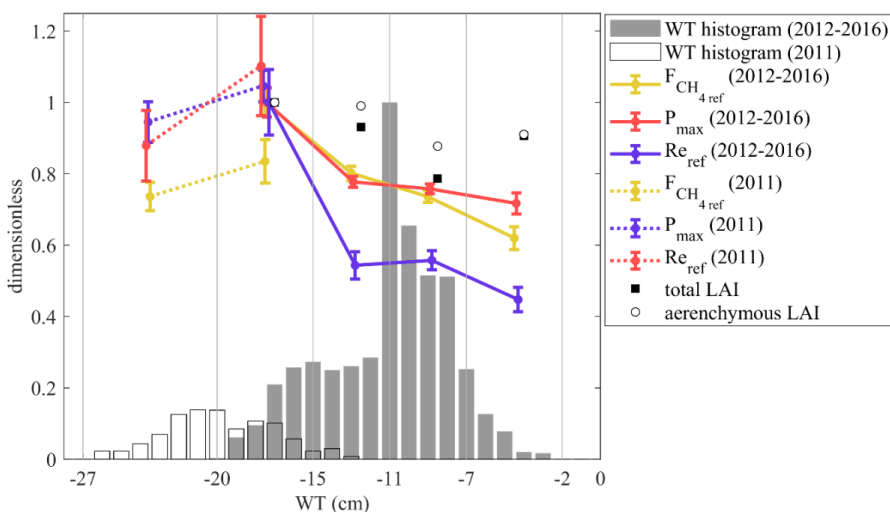
3.4.2 Response to dry and hot conditions

Figure 11: Reference fluxes for F_{CH4} and Re and maximum photosynthesis P_{max} *versus* water table depth, calculated as averages for the data within 5 WTD bins (marked by vertical lines), normalized by the value of the maximum bin-average, along with the corresponding air temperature and measured LAI bin-averages. The 2011 data are normalized by the 2012–2016 maxima, thus yielding values above unity. The data are from the period of June-August. The uncertainty bars give 50% parameter CI. The WTD histogram is shown as grey bars. WTD histograms and flux parameters are shown separately for 2011 and 2012–2016.

Our dataset includes a markedly dry period of 2011. The response of the carbon fluxes to low WTD conditions was evaluated by fitting Eqs. 4–6 in five WTD bins (Fig. 11) in order to estimate the effect of dry conditions on flux model parameters. The data of 2011 are shown separately. When WTD is less than 15 cm, P_{max}, F_{ref} and Re_{ref} do not vary with water table. When WTD is lower (-20 > WTD > -15 cm), all of them are at their maximum. The two bins representing 2011 show that at yet lower WTD (<-20 cm), the reference fluxes stagnate or are slightly reduced. The parameter values in the -20 – -15 cm bin, where the data of 2011 and 2012–2016 overlap, indicate similar P_{max} and Re_{ref} but a lower F_{ref} in 2011 compared with 2012–2016.

3.5 Drivers of the interannual variation in CO_2 and CH_4 fluxes

The cumulative growing season NEE, its components and the net CH_4 emission are summarized in Table 5. The typical summertime F_{CH4} sums up to 4.8–6.4 g C m^{-2}, and in the growing season 6.4–8.4 g C m^{-2}. The summertime Re is 100–150 g C m^{-2} and GPP about 150–200 g C m^{-2}, resulting in an May–Sep NEE of -20 to -64 g C m^{-2}. May and September make a small addition to Re and GPP, raising the average cumulative NEE from -49 C m^{-2} in Jun-Aug to -60 g C m^{-2} in May–Sep.

**Table 5:** Cumulative gap-filled summer and growing season CO_2, CH_4 fluxes and their 6-year averages, in g C m^{-2}.

	June–August	May–September

|	F_{CH4}	NEE	Re	GPP	F_{CH4}	NEE	Re	GPP
2011	5.8	-33	151	185	7.6	-47	197	244
2012	4.8	-20	125	145	6.5	-24	169	193
2013	6.4	-64	107	171	8.4	-72	156	228
2014	5.8	-57	144	201	7.3	-77	180	257
2015	4.9	-59	103	162	6.4	-70	146	216
2016	4.8	-54	114	168	6.5	-72	157	229
6-year average	5.4	-49	124	173	7.1	-60	167	228

We attempted to estimate the uncertainty of cumulative fluxes by comparing the results of the above gap-filling method (Sect.

380   2.4) with those that were eventually discarded. The different gap-filling methods led to a relative variation of some tens of g C m^{-2} in Re and GPP, and about 0.5 g C m^{-2} in F_{CH4}. In the year 2013 having the worst data coverage (Table 1), the cumulative GPP estimates by different gap-filling methods ranged between 190 and 270 g C m^{-2} (i.e. up to 20% relative uncertainty on the average of 235 g C m^{-2}), while in the rest of the years the range was much smaller (20-30 g C m^{-2} around the average GPP, or about 10%). These relative uncertainties in GPP and Re, however, aggregate to a rather high relative uncertainty on May-Sep

385   cumulative NEE which may be estimated at 30-40%. The uncertainty of cumulative NEE for 2013 alone is difficult to gauge; it may approach 100% so the small net cumulative C uptake is not statistically significant. However, it is a likely result and is treated as such in the following. Given these considerations, the seasonal cumulative values presented in Table 5 should be taken with caution as they contain a large proportion of gap-filled data. We chose to use these values for general reference only, and conduct the further analysis exclusively on the mean instantaneous fluxes.

390   The year-to-year variability of the measured fluxes strongly correlates with the interannual variability of some environmental parameters (Fig. 12). High air and peat temperature favor high GPP, Re and F_{CH4}. At the same time, high fluxes correspond to low WTD and high VPD. This suggests that the CO_2 fluxes and methane emission are temperature-controlled, and the dry conditions associated with warm weather do not impose strict limitations. This is true as long as the WTD is not very low, as shown in Fig. 11 – but such dry periods did not last long enough to drastically affect the seasonal balances. In fact, the negative

395   impacts are detectable in the two years representing the opposite extremes – hot and dry 2011 and cool and moist 2012. In both years, the summer and growing season NEE was reduced compared with the other years. In line with some previous studies (e.g. Rinne et al. 2018), the cumulative GPP and F_{CH4} values are found to be positively correlated (Fig. 13a). In addition, F_{CH4} shows a saturating behavior at increasing Re (Fig. 13c).

Biogeosciences
Discussions

Open Access
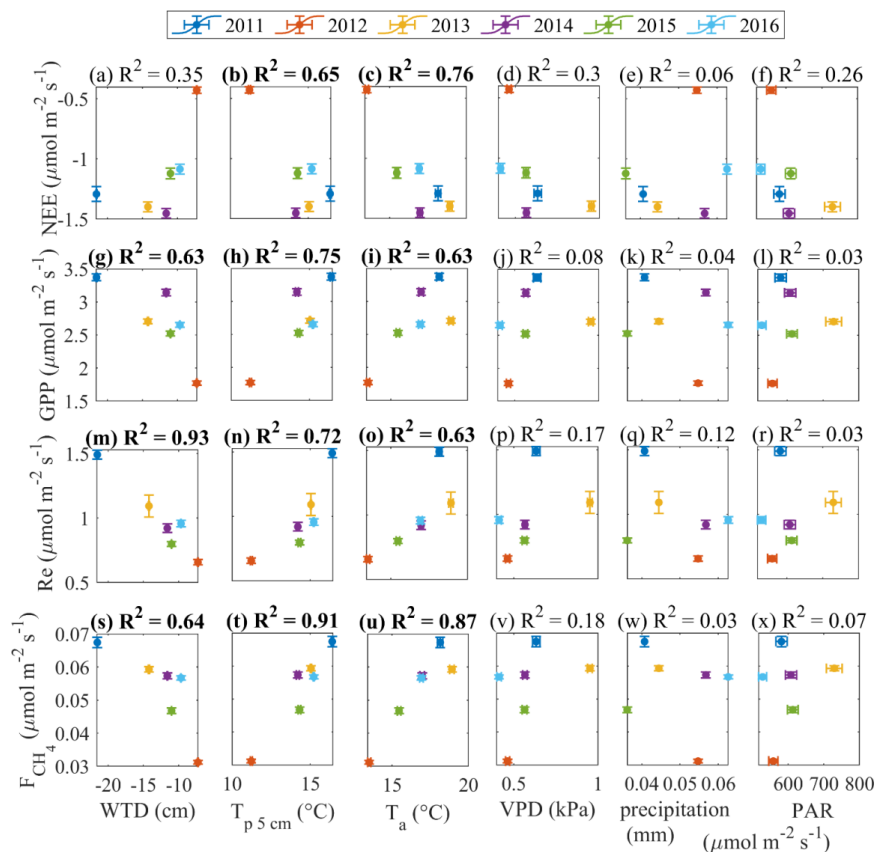
Figure 12: May-Sep mean measured fluxes versus averages (or cumulative, in the case of precipitation) of environmental drivers. R^2 values >0.6 are shown in bold.
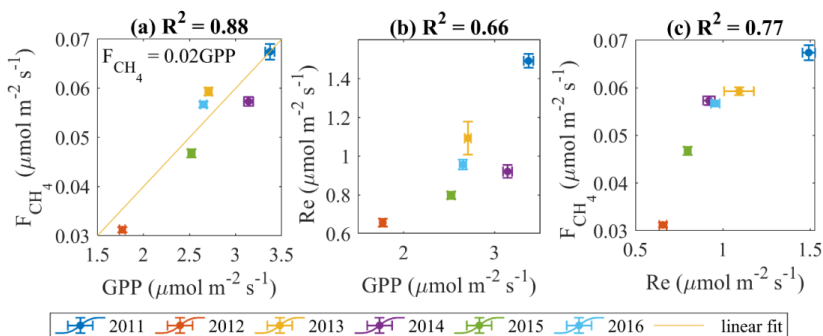
Figure 13: Relationships between the mean measured May-Sep fluxes.

4. Discussion

4.1 Filtering for low turbulence conditions

The friction velocity threshold was evaluated from the relationship with EC CO_2 flux and F_{CH4}. As this method uses all available F_{CH4} data, but only nighttime CO_2 flux data, given equal random uncertainties one may hypothesize that using F_{CH4} leads to a

410   better-defined threshold. Here, the two thresholds, matched – as they should have, owing to identical aerodynamic transport for scalars. However, the fact that the energy balance closure deficit continues into higher u_* implies the presence of some other factors degrading the performance of EC technique, which might be related to poor representativeness of the footprint, or importance of storage fluxes. This observation calls for wider application of alternative strategies to EC flux filtering, and a more critical approach to the standard u_* filtering method.

415   ### 4.2 Average growing season carbon exchange

The Siikaneva-2 bog was a net CO_2 sink and CH_4 source in each of the six growing seasons. The cumulative growing season (May–September) Re averaged 171 g C m^{-2} and GPP 228 g C m^{-2}, yielding an NEE of -57 g C m^{-2}. These are similar to the results in other bog studies. For instance, middle taiga bog uptake measured near the Zotino station was between 40–60 g C m^{-2} between April and October in three years (Arneth et al. 2002). Cumulative May–August NEE of 66–107 g C m^{-2} was found by

420   Humphreys et al. (2014) over two years in three Canadian bogs (Attawapiskat River, Kinoje Lake and Mer Bleu). Attawapiskat River and Kinoje Lake in Hudson Bay Lowlands are on par with Siikaneva-2, having May-August Re of about 160–170 g C m^{-2}, GPP of 220–240 g C m^{-2} and NEE of 60–70 g C m^{-2}. The shrub bog Mer Bleu produced an NEE of 88–107 g C m^{-2} with Re of 378–432 g C m^{-2} and GPP or 466–539 g C m^{-2}.

The cumulative CH_4 efflux in Siikaneva-2 averaged 7.2 g C m^{-2}, which is slightly higher than the 3.6–4.6 g C m^{-2} reported by

425   Vompersky et al. 2000 based on a growing season measurement campaign (184 days in May–October) on a south taiga ridge-hollow complex in European Russia. A much higher annual release of CH_4 (19.5 g C m^{-2}) was observed by Friborg et al. (2003) at the Plotnikovo site in the Bakchar bog (south taiga). A Canadian temperate shrub bog showed a 6-year average annual CH_4 emission of 3.7±0.5 g C m^{-2} (Roulet et al. 2007).

The cumulative fluxes in Siikaneva-2 were close to those presented by Rinne et al. (2018) for the fen site Siikaneva-1 which is

430   situated 1.3 km ESE of Siikaneva-2. There, an NEE of similar magnitude was realized via Re and GPP approximately 200 g C m^{-2} higher than those in Siikaneva-2 (Rinne et al. 2018). At the same time, the methane emission is about 25% lower in Siikaneva-2 bog than in Siikaneva-1 fen, estimating as the average ratio of the measured 30-min EC CH_4 fluxes.

4.3 Drivers of interannual variability

The interannual differences in cumulative GPP, Re and CH_4 emission were mainly controlled by temperature, with all fluxes

435   increasing in warmer conditions. In a year without positive or negative precipitation extremes, this leads to a rather stable May–Sep NEE of about -70 g C m^{-2}. In a year with ample precipitation, high WTD and low PAR (2012) this dropped to about -24 g C m^{-2} (highly uncertain due to poor data coverage). In a year with a hot dry summer (2011), a moderately reduced May–Sep NEE of -47 g C m^{-2} was observed.

The driest summer on record (2011) neither converted the peatland into net CO_2 source, nor did it arrest the CH_4 emission. This

440   resilience seems to hold as long as the water table depth is above a threshold value, which is presumably at about -20 cm at this site (Fig. 13). Below that level, the reference fluxes cease increasing, implying that the positive effects of higher peat

temperature have become balanced by the negative effect of dryness. However, the dry period of 2011 seems to have caused only a small decline in NEE, even though the WTD resided about 10 cm lower than the seasonal average for several weeks in a row. As warm summers clearly create conditions for high GPP, the reduction of NEE during drought is maybe more due to

445 enhancement of respiration rather than suppression of photosynthesis. Strong enough drought can cause annual net CO_2 emission from bogs, however. Alm et al. (1999) report net release of carbon in a dry year at an open *Sphagnum* bog in eastern Finland, where NEE amounted to +80 g C m^{-2} (GPP = 205 g C m^{-2}, Re = 285 g C m^{-2}), with most of the loss occurring on hummocks, while lawns remained nearly C-neutral. In a Swedish temperate bog, Lund et al. (2012) observed near-zero annual average NEE due to drought in two out of fours measurement years. A temperate bog became a considerable net source of CO_2 (Arneth et al.

450 2002). An apparently saturating behavior of F_{CH4} as a function of Re (Fig. 13c) is another indication of GHG emission rebalancing in dry conditions: as Re is enhanced, F_{CH4} stagnates. Our results reinforce the view that only a strong drought is able to nullify net growing season CO_2 sink and strongly reduce CH_4 emission of a boreal bog. The drought timing may be important as well – hypothetically, an early spring drought may hamper the development of deciduous (shrub, graminoid) plant biomass, and so limit photosynthesis and CH_4 emission for the rest of the summer; conversely, a drought initiated after the plant biomass

455 has developed would have a lesser effect since the leaf area and the roots are already present and the vegetation has acquired a degree of resilience. This dynamics could have been in action at the Fäjemyr temperate bog, where a long and early drought lowered both GPP and Re, while a drought that started later in another year only increased Re (Lund et al. 2012)

A different set of limitations in 2012, now probably through low temperature and PAR, caused a stronger reduction in net CO_2 sink than in 2011. The cumulative NEE went down by about 50 g C m^{-2}, or about 70% compared to 2013–2016. The growing

460 season cumulative F_{CH4} at 6.5 g C m^{-2} was at the low end, although nearly identical to the emission in 2015 and 2016. This observation suggests that lowered air temperature and overcast conditions are a stronger limiting factor to plant growth and CH_4 emission than moderately hot and dry conditions. A reduction in solar radiation during daytime overcast/rainy weather limits photosynthesis (Nijp et al. 2015). It is difficult to tell if the elevated WTD imposed a direct limitation on GHG production or transport. limits Previous studies show wet conditions without reduction in temperature result in high bog CO_2 uptake. Friborg et

465 al. 2003 estimated net CO_2 uptake of -108 g C m^{-2} year^{-1} in Bakchar bog, South taiga. May-August NEE of -202 g C m^{-2} was observed in a wet year with a warm spring in the Mukhrino bog in Siberian middle taiga by Alekseychik et al. 2017; dry weather in the following year resulted in significantly lower net uptake due to higher Re and lower GPP at their west Siberian site (unpublished data). European south taiga bog Fyodorovskoye had a similar weather sensitivity, being a sink of 60 g C m^{-2} in a wet year compared with a source of 25 g C m^{-2} in a dry year (Arneth et al. 2002). As a side note, carbon leaching may have been

470 higher as ample precipitation must have boosted runoff, and may have thus removed DOC which may have otherwise contributed to heterotrophic respiration and CH_4 emission; Roulet et al. 2007 estimated an annual average net carbon leaching of 14.9 ± 3.1 g m^{-2}, roughly one third of the NEE observed in our study.

If the plants are expected to drive CH_4 emission, LAI and F_{CH4} should be well correlated on a seasonal scale with closely matching peaks. This, in fact, is partly confirmed by the analysis seasonal peaks timing (Fig. 8). While LAI and GPP are in-

475 phase (Fig. 8), the magnitudes of their peaks in the individual years were not correlated (not shown), meaning that LAI might contribute to the seasonal shape of F_{CH4} but does not determine its seasonal peak. Regarding the peak in F_{CH4}, its occurrence between those in LAI and T_{p20} is an independent indication that both controls might be important. The linear correlation between GPP and F_{CH4} (Fig. 13a) comes as no surprise, as both become enhanced in warm conditions (Fig. 12), but it was not possible to check if this reflects causality of just a similar reaction to environmental factors. With the present dataset, it was not possible to

480 confirm the plant contribution to methanogenic substrate and CH_4 transport. However, a pulse-labelling study of Dorodnikov et al. (2011) showed that recent photosynthates (on the time-scale of a few hours to a few days) made a minuscule contribution to

the total CH_4 emission, whereas transport through *Eriophorum vaginatum* and *Scheuchzeria palustris* amounted to 30–50% of the total methane efflux. Consequently, the apparent relationship between F_{CH4} with Net Ecosystem Productivity (NEP) might simply be due to the direct link between Leaf Area Index (LAI) and NEP. Curiously, the slope of the GPP-F_{CH4} linear
485 relationship in Fig. 13a, 0.021 (CI 0.01–0.032) is significantly lower than 0.06 reported by Rinne et al. (2018) for the June– September period in a nearby fen, which might be related to the fact that sedges, the genus usually found to enhance CH_4 emission, make up a larger fraction of GPP at the fen site.

4.4 Drivers of the seasonal CO_2 and CH_4 exchange

The carbon flux model parameters, resolved in time, display pronounced seasonal courses. The reference flux of respiration,
490 Re_{ref}, peaks distinctly in May–June (Fig. 7a), which is clearly too late to indicate the release of CO_2 stored during the snow-on period. There is a secondary Re_{ref} peak later in October. F_{ref} is expectedly at the maximum in April–early May, at the time of snowmelt, whereas a weak correlation with LAI persists in the growing season (Fig. 7b). The autumn peaks in F_{ref} are interesting, as they are not exactly correlated with those in Re_{ref}; transport through the sedge stems or peat freezing pushing out the bubbles are the potential mechanisms explaining the increased CH_4 flux (e.g. Whiting and Chanton 1992). P_{max} has a well-defined bell-
495 shaped seasonal course (Fig. 7c), with the peak coinciding with the maximum LAI, T_a, T_p and the lowest WTD (Fig. 8). The seasonality of k is similar to that of P_{max}, albeit with more scatter.

It was difficult to explain the short-term (under 1 month) variation in the four model parameters. To large extent this is due to random uncertainty and gaps in the EC flux data, but results also partly from the change in footprint and domination of plant species known to have different light photosynthetic light response and phenology (Korrensalo et al. 2017). The strongest
500 positive correlation is found between P_{max} and T_{p5}, on a biweekly time scale; this should be seen in connection to the fact that the GPP model involving T_{p5} showed the best performance.

Despite rather incomplete temporal coverage, we attempted to evaluate the importance of the non-growing season fluxes. The magnitude of the spring peak was quite small, supplying about 4% to the summertime CH_4 emission in both years when it was measured. Rinne et al. (2018) found a similarly small spring peak that was absent in some years. The late autumn and winter
505 fluxes, however, did contribute substantially (>10%) to the May-October or May-December Re and F_{CH4}, but less so to GPP (<5%).

Variations in WTD seem to cause substantial variability in the flux model parameters (Fig. 11). What might cause such a peak in CH_4 and CO_2 reference fluxes at a low WTD? The air temperature varies significantly across the bins, but LAI stays constant. As the positive effect of T_a on GPP is known, the P_{max} maximization at the warmest temperatures is expected, as long as moisture
510 supply is not disrupted. In contrast, the Re and F_{CH4} reference fluxes are independent of temperature by virtue of their formulation. This leaves us to hypothesize that it is the photosynthesis per leaf area, expressed here via its proxy, P_{max}, which causes similar responses of F_{ref} and Re_{ref} to WTD. The fact that all three parameters get saturated only at a rather low WTD provides a hint as to why a large reduction in GPP, respiration and methane efflux is not observed in moderately dry and hot years. Lafleur et al. (2005) observed insensitivity of Re to WTD at the Mer Bleu shrub bog. At the same time, a lowered water
515 table position is typically shown to be a negative effect on mire CH_4 emission (e.g. Glagolev et al. 2001a, Kalyuzhny et al. 2009); however Rinne et al. (2018) propose the existence of an optimum WTD range (approx. -30…0 cm) maximizing the CH_4 efflux in a fen Siikaneva-1 (SI1) close to the bog Siikaneva-2.

4.5 EC Footprint variation effect

The actual EC source area is uncertain, as footprint models of Kormann & Meixner (2001) and Kljun et al. (2015) provided
520   contrasting results regarding the footprint length (Fig. 3). Nonetheless, The EC data can be considered representative of the bog
ecosystem, given the similarity between the cumulative footprint-weighted surface contributions and their abundance within the
wider area (Table 2). The footprints had significantly different lengths, the Kljun et al. (2015) model yielding shorter footprints.
This is fully consistent with the results of Arriga et al. (2017) who observed the same relationship, and found that the true source
is between the estimates of the two models. Nevertheless, the variability in surface types between wind sectors is apparently
525   more important than the variation with distance from the EC tower, because the surface type contributions calculated using the
two models are very similar (Table 2). In such a heterogeneous site as Siikaneva bog, the directional variation in the microform
contributions to EC flux does not come as a surprise (Fig. 9). The amplitude of variation in the lawn, mud bottom and pond
contributions reaches 10–20%; curiously, the K&M and Kljun models agree on this, despite differing on footprint length. Maybe
of greatest interest are the directional differences in the pond contribution, with the maximum in 230˚–N–30˚ and minimum at
530   50˚–200˚. In a similarly heterogeneous tundra site, Tuovinen et al. (2019) found that the variation of the EC footprint with
stability and wind direction induced a significant bias between the EC flux and the "true" upscaled flux of the region.
Nevertheless, the cumulative contributions of the different microforms to the EC flux were close to their fractions over the 400 x
400 area centered at the EC tower, implying that the EC data are representative of the ecosystem-average fluxes.

The question is now: is the effect of the ponds on the EC fluxes discernible, even despite their contribution varying with wind
535   direction from 0% to a maximum of 20% depending on wind direction? In case the microforms have widely different C
exchange rates, the footprint variation effect should, in principle, be discernible. Earlier chamber studies suggest that CH_4 efflux
from microtopography elements with lower elevation (hollows) is higher than that from ridges/hummocks (e.g. Glagolev and
Suvorov 2007, Glagolev and Shnyrev 2008, Maksuytov et al. 2010). Alm et al. 1999 observed annual CH_4 fluxes ranging from 2
g C m^{-2} on hummocks to 14 g C m^{-2} on hollows. High CH_4 emission was detected on ponds (Repo et al. 2007, Maksuytov et al.
540   2010) and float mats (Kazantsev et al. 2010). However, chamber studies in Siikaneva-2 bog didn't find significant differences in
CH_4 efflux on different microforms (Korrensalo et al. 2017). Nevertheless, the EC data do show that both the normalized F_{CH4}
and the F_{CH4} reference flux were actually elevated within the sector with the maximum pond contribution (Fig. 10). This apparent
emission peak occupies only a part of the sector containing the ponds, meaning that either the individual ponds emit different
amounts of CH_4, or the anomaly is not related to ponds at all. The existence of the CH_4 emission hotspot is independently
545   confirmed by comparison of the chamber fluxes across the chamber plots located to the west, east and north of the EC tower; the
western sector CH_4 chamber flux is the highest (Aino Korrensalo, personal communication). The effect of ebullition may be
ruled out based on the results of Männistö et al. (2019), who studied the variation of ebullitive CH_4 flux from vegetation-free
surfaces (ponds, pond edges, mud bottoms) and estimated that the relative growing season contribution of the ebullition on these
surfaces to the integrated EC-scale flux amounts to 3–5%. Boardwalks and other station infrastructure are concentrated in the W
550   and NE sectors (Fig. 9), and appear to correlate with the CH_4 peak in the W sector (Fig. 10). However, the "boardwalks" share is
an overestimate due rescaling the original aerial images to the map at the resolution of 1 x 1 m. Second, the disturbance of peat
due to the presence of boardwalks or chamber collars and their use certainly played no role here, as the CH_4 emission hotspot had
been present in 2011, before any infrastructure was built in the western sector. The drop in GPP and P_{max} in the same sector is
logical: less area covered by plants in the "pond" sector logically leads to lower photosynthesis. This supports the idea of the
555   potential pond origin of the elevated CH_4 emission.

Re and Re_{ref} were significantly higher in the sector 0˚–130˚ than in 150˚–300˚, possibly due to the higher contribution of
hummocks and lower WTD in the NE sector (see also Korrensalo et al. 2017).

Biogeosciences
Discussions

Open Access

EGU

5 Conclusions

560 The growing season CO_2 and CH_4 cumulative fluxes in the southern Finnish bog Siikaneva-2 are similar to the previous estimates for other boreal bogs. The 6-year average May-September NEE is -57 g C m^{-2}, which splits into 171 g C m^{-2} of Re and 228 g C m^{-2} of GPP, whereas the cumulative net CH_4 efflux is 7.2 g C m^{-2}. The variation in cumulative Re, GPP and F_{CH4} were correlated with the average air and peat temperatures, while water table level was not a limiting factor except in the driest of periods, which were too short to affect the seasonal balances. However, it proved difficult to separate the effects of the flux drivers due to their strong mutual dependency. The growing season cumulative GPP was well correlated with F_{CH4}, as in the

565 nearby fen (Rinne et al. 2018). The non-growing season fluxes were not negligible, and need to be reassessed in future studies. However, this mostly relates to autumn and early winter, as the early spring photosynthesis was low and the spring F_{CH4} peak noticeable but its contribution was minor on the annual timescale.

Even in such a strongly patterned site, the surface heterogeneity was insufficient to demonstrate conclusively any footprint-related variations in EC fluxes. The upwind GHG sources were well integrated by the EC method, and there was not enough

570 directional difference in surface cover. As a result, the contributions of the different surfaces did not vary with wind direction by more 10–20%, which is too small considering the joint uncertainties in the footprint model, microform map and EC fluxes. The dependency of P_{max} on the ratio of vegetated/non-vegetated surfaces in footprint was the only signal of surface heterogeneity in agreement with the known EC footprint composition. EC CH_4 flux peaked in the western sector, possibly due to higher proportion of ponds and higher WTD in that sector, but no correlation with the surfaces contributing to the EC flux was found.

575 The complications with the interpretation of the EC data encountered in this study stem from highly correlated changes of the environmental drivers and the flux footprint, on the timescales from week to season. These limitations apply to all eddy-covariance sites, which calls for a more critical approach to EC data interpretation and modeling.

Code availability

The codes used in the preparation of this manuscript are available upon request from the authors.

580 Data availability

The data used in the preparation of this manuscript are available upon request from the authors.

Author contribution

Competing interests

The authors declare no competing interests.

590 Acknowledgements

References

Alekseychik, P., Mammarella, I., Karpov, D., Dengel, S., Terentieva, I., Sabrekov, A., Glagolev, M., and Lapshina, E.: Net ecosystem exchange and energy fluxes measured with the eddy covariance technique in a western Siberian bog, Atmos. Chem. Phys., 17, 9333–9345, https://doi.org/10.5194/acp-17-9333-2017, 2017.

600   Alm, J., Saarnio, S., Nykänen, H., Silvola, J. and Martikainen, P.J.: Winter CO2, CH4 and N2O fluxes on some boreal natural and drained peatlands, Biogeochemistry, 44, 163–186., 1999.

Arneth, A., Kurbatova, J., Kolle, O., Shibistova, O. B., Lloyd, J., Vygodskaya, N. N., and Schulze, E.-D.: Comparative ecosystem–atmosphere exchange of energy and mass in a European Russian and a central Siberian bog II. Interseasonal and interannual variability of CO2 fluxes, Tellus B, 54, 514–530, https://doi.org/10.3402/tellusb.v54i5.16684, 2002.

605   Arriga, N., Rannik, Ü, Aubinet, M., Carrara, A., Vesala, T., and Pa-pale, D.: Experimental validation of footprint models for eddycovariance CO2flux measurements above grassland by means ofnatural and artificial tracers, Agr. Forest Meteorol., 242, 75–84,2017.

Aubinet, M., Vesala, T., and Papale, D. (Eds.): Eddy covariance: a practical guide to measurement and data analysis, Springer Science & Business Media, Berlin, Germany, 2012.

610   Baldocchi, D. D.: 'Breathing' of the terrestrial biosphere: lessons learned from a global network of carbon dioxide flux measurement systems, Austr. J. Bot., 56, 1–26, 2008.

Bellisario, L. M., Bubier, J. L., Moore, T. R., and Chanton, J. P.: Controls of CH4emissions from a northern peatland, Global Biogeo-chem. Cycles, 13, 81–91, 1991.

Buttler. A., Robroek, B.J.M., Laggoun-Défarge, F., Jassey, V.E.J., Pochelon, C., Bernard, G., Delarue, F., Gogo, S., Mariotte, P.,
615   Mitchell, E.A.D., and Bragazza, L.: Experimental warming interacts with soil moisture to discriminate plant responses in an ombrotrophic peatland, Journal of Vegetation Science 26, 964–974. https://doi.org/10.1111/jvs.12296, 2015.

Charman, D.J., Beilman, D.W., Blaauw, M., Booth, R.K., Brewer, S., Chambers, F.M., Christen , J.A., Gallego-Sala, A., Harrison, S.P., Hughes, P.D.M., Jackson, S.T., Korhola, A., Mauquoy, D., Mitchell, F.J.G., Prentice, I.C., van Der Linden, M., De Vleeschouwer, F., Yu, Z.C., Alm, J., Bauer, I.E., Corish, Y.M.C., Garneau, M., Hohl, V., Huang, Y., Karofeld, E., Le Roux,
620   G., Loisel, J., Moschen, R., Nichols, J.E., Nieminen, T.M., MacDonald, G.M., Phadtare, N.R., Rausch, N., Sillasoo, Ü., Swindles, G.T., Tuittila, E.S., Ukonmaanaho, L., Väliranta, M., van Bellen, S., van Geel, B., Vitt, D.H., and Zhao, Y, Climate-related changes in peatland carbon accumulation during the last millennium, Biogeosciences, 10, 929–944, 2013.

Davidson, E. A. and Janssens, I. A.: Temperature sensitivity of soil carbon decomposition and feedbacks to climate change, Nature, 440, 165–173, 2006.

625   Dorodnikov, M., Knorr, K.H., Kuzyakov, Y., and Wilmking, M.: Plant-mediated CH4 transport and contribution of photosynthates to methanogenesis at a boreal mire: a C-14 pulse-labeling study, Biogeosciences, 8, 2365–2375, 2011.

Dunfield, P., Knowles, R., Dumont, R.T., and Moore, T.R.: Methane production and consumption in temperate and subarctic peat soils: response to temperature and pH. Soil Biol. Biochem., 25, 321–326, 1993.

Biogeosciences

Discussions

Open Access

EGU

Euskirchen, E.S., Edgar, C.W., Turetsky, M.R., Waldrop, M.P., Harden, J.W.: Differential response of carbon fluxes to climate
630   in three peatland ecosystems that vary in the presence and stability of permafrost, J. Geo. Res.: Biogeosciences, 119, 1576–1595,
2014.

Fechner-Levy, E.J., and Hemond, H.F.: Trapped methane volume and potential effects on methane ebullition in a northern
peatland, Limnol. Oceanogr., 41, 1375–1383, 1996.

Friborg, T., Soegaard, H., Christensen, T. R., Lloyd, C. R., and Panikov, N. S.: Siberian wetlands: Where a sink is a source,
635   Geophys. Res. Lett., 30, 2129, https://doi.org/10.1029/2003GL017797, 2003.

Frolking, S., and Roulet, N.T.: Holocene radiative forcingimpact of northern peatland carbon accumulation and methane
emissions, Glob. Change Biol, 13, 1079–1088, doi:10.1111/j.1365-2486.2007.01339.x, 2007.

Glagolev M., Inisheva L., Lebedev V., Naumov A., Dement'eva T., Golovatskaja E., Erohin V., Shnyrev N., and Nozhevnikova
A.: The Emission of CO2 and CH4 in Geochemically Similar Oligotrophic Landscapes of West Siberia, in: Proceedings of the
640   Ninth Symposium on the Joint Siberian Permafrost Studies between Japan and Russia in 2000, Sapporo, Japan, 23-24 January,
2001, Sapporo, Kohsoku Printing Center, 112–119, 2001.

Glagolev, M.V. and Shnyrev, N.A.: Methane emission from mires of Tomsk oblast in the summer and fall and the problem of
spatial and temporal extrapolation of the obtained data, Moscow University Soil Science Bulletin 63, 67–80, 2008.

Glagolev, M.V. and Suvorov, G.G.: Methane emission from wetland soils in middle taiga (by example of Khanty-Mansi
645   autonomous district) [in Russian with English summary], Doklady po Ekologicheskomu Pochvovedeniyu, 2, 90–162, 2007.

Gorham, E.: Northern peatlands: role in the carbon cycle and probable responses to climatic warming, Ecol. Appl., 1, 182–195,
1991.

Humphreys, E. R., Charron C., Brown, M., and Jones, R.: Two bogs in the Canadian Hudson Bay Lowlands and a temperate bog
reveal similar annual net ecosystem exchange of CO2, Arct. Antarct. Alp. Res., 46, 103–113, 2014.

650   Kazantsev V.S., Glagolev M.V., Golubyatnikov L.L., Maksyutov S.S.: Methane emissions from lakes in West Siberian wetlands,
in: proceedings of the EGU General Assembly 2010, Vienna, Austria, Geophysical Research Abstracts, 12, EGU2010-358, 2010.

King, G.M., Roslev, P., and Skovgaard, H.: Distribution and rate of methane oxidation in sediments of the Florida Everglades,
Appl. Environ. Microbiol., 56, 2902–2911, 1990.

Kljun, N., Calanca, P., Rotach, M. W., and Schmid, H. P.: A simple two-dimensional parameterisation for Flux Footprint
655   Prediction (FFP), Geosci. Model Dev., 8, 3695–3713, https://doi.org/10.5194/gmd-8-3695-2015, 2015.

Kormann, R. and Meixner, F. X.: An Analytical Footprint Model For Non-Neutral Stratification, Bound.-Lay. Meteorol., 99,
207– 224, https://doi.org/10.1023/a:1018991015119, 2001.

Korrensalo, A., Alekseychik, P., Hájek, T., Rinne, J., Vesala, T., Mehtätalo, L., Mammarella, I., and Tuittila, E.-S.: Species-
specific temporal variation in photosynthesis as a moderator of peatland carbon sequestration, Biogeosciences, 14, 257–269,
660   https://doi.org/10.5194/bg-14-257-2017, 2017.

Korrensalo, A., Hájek, T., Vesala, T., Mehtätalo, L., and Tuittila, E-S.: Variation in photosynthetic properties among bog plants,
Botany, 94, 1127–39, 2016.

Korpela, I., Haapanen, R., Korrensalo, A., Tuittila, E.-S., Vesala, T.: Fine-resolution mapping of microforms of a boreal bog
using aerial images and waveform-recording LiDAR. *Mires and Peat*, 26, 03, doi:10.19189/MaP.2018.OMB.388, 2020.

665   Lai, Y. F.: Methane dynamics in northern peatlands: A review, Pedosphere, 19, 409–421, 2009.

Laine, A. M., Mäkiranta, P., Laiho, R., Mehtätalo, L., Penttilä, T., Korrensalo, A., Minkkinen, K., Fritze, H., and Tuittila, E-S.:
Warming impacts on boreal fen CO2exchange under wet and dry conditions, Global ChangeBiol, 25, 1995–2008.
doi:10.1111/gcb.14617, 2019.

Lafleur, P. M., Moore, T. R., Roulet, N. T., and Frolking, S.: Ecosystem respiration in a cool temperate bog depends on peat

670   temperature but not on water table, Ecosystems, 8, 619–629, doi:10.1007/s10021-003-0131-2, 2005.

Lafleur, P. M., Roulet, N. T., Bubier, J. L., Frolking, S., and Moore, T. R.: Interannual variability in the peatland-atmosphere carbon dioxide exchange at an ombrotrophic bog, Global Biogeochem. Cy., 17, 1036, 1036https://doi.org/10.1029/2002gb001983, 2003.

Lund, M., Christensen, T. R., Lindroth, A., and Schubert, P.: Effects of drought conditions on the carbon dioxide dynamics in a

675   temperate peatland, Environmental Research Letters, 7, 045704, https://doi.org/10.1088/1748-9326/7/4/045704, 2012.

Lund, M., Lafleur, P. M., Roulet, N. T., Lindroth, A., Christensen, T. R., Aurela, M., Chojnicki, B. H., Flanagan, L. B., Humphreys, E. R., Laurila, T., Oechel, W. C., Olejnik, J., Rinne, J., Schubert, P., and Nilsson, M. B.: Variability in exchange of CO2 across 12 northern peatland and tundra sites, Glob. Change Biol., 16, 2436–2448, doi:10.1111/j.1365-2486.2009.02104.x, 2010.

680   Lund, M., Lindroth, A., Christensen, T. R. and Ström, L.: Annual CO2 balance of a temperate bog, Tellus B, 59, 804–11, 2007.

Maksyutov, S., Glagolev, M., Kleptsova, I., Sabrekov, A., Peregon, A., and Machida, T.: Methane emissions from the West Siberian wetlands, in: proceedings of the American Geophysical Union Fall Meeting 2009, San Francisco, USA, abstract #GC41D-02, 2010.

Mammarella, I., Peltola, O., Nordbo, A., Järvi, L., and Rannik, Ü.: Quantifying the uncertainty of eddy covariance fluxes due to

685   the use of different software packages and combinations of processing steps in two contrasting ecosystems, Atmos. Meas. Tech., 9, 4915–4933, https://doi.org/10.5194/amt-9-4915-2016, 2016.

Männistö, E., Korrensalo, A., Alekseychik, P., Mammarella, I., Peltola, O., Vesala, T., and Tuittila, E.-S.: Multi-year methane ebullition measurements from water and bare peat surfaces of a patterned boreal bog, Biogeosciences, 16, 2409–2421. https://doi.org/10.5194/bg-16-2409-2019, 2019.

690   Nemitz, E., Mammarella, I., Ibrom, A., Aurela, M., Burba, G., Dengel, S., Gielen, B., Grelle, A., Heinesch, B., Herbst, M., Hörtnagl, L., Klemedtsson, L., Lindroth, A., Lohila, A., McDermitt, D.K., Meier, P., Merbold, L., Nelson, D., Nicolini, G., Nilsson, M.P., Peltola, O., Rinne, J., and Zahniser, M.: Standardization of eddy covariance flux measurements of methane and nitrous oxide, Int. Agrophys., 32, 517-549, doi: 10.1515/intag-2017-0042, 2018.

Nijp, J.J., Limpens, J., Metselaar, K., Peichl, M., Nilsson, M.B., Van Der Zee, S.E.A.T.M., and Berendse, F. Rain events

695   decrease boreal peatland net CO$_2$ uptake through reduced light availability, Global Change Biology, 21, 2309– 2320, 2015.

Pirinen P., Simola, H., Aalto, J., Kaukoranta, J., Karlsson, P. and Ruuhela, R.: Tilastoja Suomen ilmastosta 1981–2010 — Climatological statistics of Finland 1981–2010. Finnish Meteorological Institute, Raportteja — Rep-porter — Reports 2012, 2012.

Rinne, J., Tuittila, E.-S., Peltola, O., Li, X., Raivonen, M., Alekseychik, P., Haapanala, S., Pihlatie, M., Aurela, M., Mammarella,

700   I., & Vesala, T.: Temporal variation of ecosystem scale methane emission from a boreal fen in relation to temperature, water table position, and carbon dioxide fluxes, Global Biogeochem. Cy., 32, 1087–1106, 2018.

Repo, M. E., Huttunen, J. T., Naumov, A. V., Chichulin, A. V., Lapshina, E. D., Bleuten, W, and Martikainen, P. J.: Release of CO2 and CH4 from small wetland lakes in western Siberia, Tellus B, 59, 788– 796, 2007.

Roulet, N.T., Lafleur, P.M., Richard, P.J.H., Moore, T.R., Humphreys, E.R. and Bubier, J.: Contemporary carbon balance and

705   late Holocene carbon accumulation in a northern peatland, Glob. Change Biol., 13, 397–411, 2007.

Sabbatini, S., Mammarella, I., Arriga, N., Fratini, G., Graf. A., Hörtnagl, L., Ibrom, A., Longdoz, B., Mauder, M., Merbold, L., Metzger, S., Montagnani, L., Pitacco, A., Rebmann, C., Sedlak, P., Sigut, L., Vitale, D. and Papale, D.: Eddy covariance raw

data processing for CO$_2$ and energy flux calculation at ICOS ecosystem stations, Int. Agrophys., 32, 495-515, doi: 10.1515/intag-2017-0043, 2018.

710 Moore, T.R., DeYoung, A., Bubier, J.L., Humphreys, E.R., Lafleur, P.M., and Roulet, N.T.: A multi-year record of methane flux at the Mer Bleue Bog, southern Canada, Ecosystems, 14, 646– 657, 2011.

Seppä, H.: Mires of Finland: regional and local controls of vegetation, landforms, and long-term dynamics, Fennia, 180, 1–2, 2002.

Stocker, T.F., Qin, D., Plattner, G.-K., Alexander, L.V., Allen, S.K., Bindoff, N.L., Bréon, F.-M., Church, J.A., Cubasch, U.,
715 Emori, S., Forster, P., Friedlingstein, P., Gillett, N., Gregory, J.M., Hartmann, D.L., Jansen, E., Kirtman, B., Knutti, R., Krishna Kumar, K., Lemke, P., Marotzke, J., Masson-Delmotte, V., Meehl, G.A., Mokhov, I.I., Piao, S., Ramaswamy, V., Randall, D., Rhein, M., Rojas, M., Sabine, C., Shindell, D., Talley, L.D., Vaughan D.G., and Xie, S.-P.: Technical Summary, in: Climate Change 2013: The Physical Science Basis. Contribution of Working Group I to the Fifth Assessment Report of the Intergovernmental Panel on Climate Change [Stocker, T.F., Qin, D., Plattner, G.-K., Tignor, M., Allen, S.K., Boschung, J.,
720 Nauels, A., Xia, Y., Bex, V. and Midgley, P.M. (eds.)], Cambridge University Press, Cambridge, United Kingdom and New York, NY, USA, 2013.

Tchebakova, N., Vygodskaya, N., Arneth, A., Marchesini, L., Kurbatova, Y., Parfenova, E., Valentini, R., Verkhovets, S., Vaganov, E., Schulze, E.: Energy and mass exchange and the productivity of main Siberian ecosystems (from eddy covariance measurements). 2.Carbon exchange and productivity, Biol Bull, 42, 579–588, 2015.

725 Tuovinen, J.-P., Aurela, M., Hatakka, J., Räsänen, A., Virtanen, T., Mikola, J., Ivakhov, V., Kondratyev, V., and Laurila, T.: Interpreting eddy covariance data from heterogeneous Siberian tundra: land-cover-specific methane fluxes and spatial representative-ness, Biogeosciences, 16, 255–274, https://doi.org/10.5194/bg-16-255-2019, 2019.

Vesala, T., Kljun, N., Rannik, Ü., Rinne, J., Sogachev, A., Markkanen, T., Sabelfeld, K., Foken, T., and Leclerc, M.Y.: Flux and concentration footprint modelling: state of the art, Environmental Pollution, 152, 653–666, 2008.

730 Vompersky S.E., Kovalev A.G., Glukhova T.V., and Smagina, M.V. Emission of carbon dioxide from the surface of forest and wetland ecosystems with varying moisture content in the southern Taiga subzone and European part of Russia (Эмиссия диоксида углерода и метана с поверхности почв лесных и болотных экосистем разной увлажненности в подзоне южной тайги и Европейской территории России) (In Russian), National conference "Emission and sink of greenhouse gases in Northern Eurasia", Pushchino, Russia, 20-24th November 2000.

735 Whalen, S. C., and Reeburgh, W. S.: Methane Oxidation, Production, and Emission at Contrasting Sites in a Boreal Bog, Geomicrobiology Journal, 17, 237–251, doi:10.1080/01490450050121198, 2000.

Wilson, D., Alm, J., Riutta, T., Laine, J., Byrne, K. A., Farrell, E. P., and Tuittila, E.-S.: A high resolution green area index for modelling the seasonal dynamics of CO2 exchange in peatland vascular plant communities, Plant Ecol., 190, 37–51, 2007.

Zhang, Z., Zimmermann, N. E., Stenke, A., Li, X., Hodson, E. L., Zhu, G., Huang, C., and Poulter, B.: Emerging role of wetland
740 methane emissions in driving 21st century climate change, Proceedings of the National Academy of Sciences of the United States of America, 114, 9647– 9652, https://doi.org/10.1073/pnas.1618765114, 2017.